Super Resolution Stripmap SAR

Christoph H. Gierull, Senior Member, *IEEE*, Ishuwa Sikaneta, Member, *IEEE*

***Abstract*—By presenting the design, configuration and required signal processing, this letter proposes a system for improved SAR imaging. Compared to conventional Spotlight SAR, the proposed system will generate imagery with equivalent or better resolution and significantly increased area coverage. The design and configuration are based upon a phased-array antenna in combination with the appropriate hardware to enable rapid electronic beam steering and to permit digitisation of multiple receive channels. The current state of technology is mature enough to construct all components of such a system. As a specific goal, the letter proposes a system capable of imaging with 10 cm resolution, a swath width of around 20 km and unlimited azimuth extent.**

I. Introduction

This letter proposes a system for improved space-based SAR imaging. It describes the design[1], which is based upon a phased-array and an appropriate switching network to allow digitisation of multiple receive channels, the configuration[2], which imposes a rapid electronic beam switching capability upon the design, and the required signal processing algorithm to compute the high definition imagery. The proposed configuration permits measurement in a stripmap-like mode, thereby offering, theoretically, unlimited azimuth extent.

The proposed approach significantly increases the area coverage (both in swath and azimuth extent) for the highest resolution imagery sensors on the commercial market while at the same time offering equivalent or better azimuth resolution. Table I highlights the added value of the approach by comparing the swath width to azimuth resolution ratio for several active commercial SAR missions [1], [4], [7], [6]. To summarise, the potential ratio of swath-width to azimuth resolution is, approximately, an order of magnitude better. In addition, the strip-like nature of the proposed configuration allows imaging over an unlimited along-track (azimuth) extent. For most commercial SAR missions the Spotlight imagery footprint in ground-range and azimuth is approximately square [6].

TABLE I
Swath width, azimuth resolution and their ratio

	Azimuth resolution (m)	**Swath width (km)**	**ratio**
RADARSAT-2	0.8	18	22.5
TerraSAR-X	0.25	4	16
CSK	0.35	7.3	22.8
Proposed	0.1	22	220.0

[1]In this letter, the design is the phased array, including its dimension and element spacing, the required switching/routing circuits, the required digitizers, and the required hardware to permit changing the transmit and receive beam table on a pulse by pulse basis.

[2]The configuration is the way in which the system is operated and includes the pulse-repetition frequency and the transmit/receive beam tables at each pulse.

The promise of such a capability, no doubt, raises questions about what unfavourable aspects of the system are amplified. What trades need to be made to realise such a system, are they physically feasible, and are they worth the reward?

For a start, imaging a larger area while maintaining a useful Signal-to-Noise-Ratio (SNR) requires a proportional increase in transmit/receive power. To avoid this problem, the size of the proposed system is on the order of 20m which is larger than most current missions (with the exception of RADARSAT-2). Also, as we shall see, the operating configuration benefits from the use of the entire receive aperture to maximise capture of scattered energy. Second, to function as specified, the operating configuration calls for the ability to transmit different beams from pulse to pulse thus requiring a rapid electronic steering capability. Third, the system needs a switching mechanism that distributes the receive sub-arrays to a multitude of distinct digitizers which, on the one hand increases hardware complexity and on the other hand, demands that more data is captured. Fourth, as the desired resolution decreases, the required azimuth beamwidth increases which also means the Doppler bandwidth increases. So, not only is the synthetic aperture physically longer (range times beamwidth), but it has to be sampled more frequently (higher bandwidth) to meet the Nyquist criteria; thus, as a rule of thumb, the required number of samples to cover the Synthetic Aperture in azimuth grows as $1/\delta_0^2$, where δ_0 is the desired azimuth resolution. As an example, while the synthetic aperture of a 3m mode on RADARSAT-2 might require $2,000$ azimuth samples, equivalent 1m and 0.1m modes would require $18,000$ and $1,800,000$ samples respectively. To make this even more challenging, depending on the used pulse waveform and on-board processing, a similar constraint would also apply in the range direction. These data need to find a path to the ground either through a link with increased bandwidth or by a mechanism that transmits less data over a longer period of time. Finally, the transformation of these more complex data into final image products requires the development and implementation of more complex signal-processing algorithms.

The next section introduces the operating configuration under ideal conditions to aid in conveying the operating concept. The combination of this operating configuration with a desired azimuth resolution dictates the design parameters and defines the minimum PRF through which the maximum swath is determined.

II. Multi-channel design and configuration

Instead of beam spoiling or spotlighting, this letter proposes an operating configuration that time-multiplexes a sequence of beams using an $M+1$ multichannel design, as illustrated in 1 (with a five-channel system). This design can be realised

with a phased-array that has the ability to change transmit and receive beam tables on a pulse by pulse basis [2], [8]. Additionally, $M+1$ digitizers and a switching mechanism to route and combine the measurements from each phased-array element (i.e. form subarrays) are required to realise this multichannel system. Although in this letter we shall consider a general $M+1$ channel system, we shall occasionally choose specific values of M for illustrative purposes. The proposed system is also a uniform antenna array.

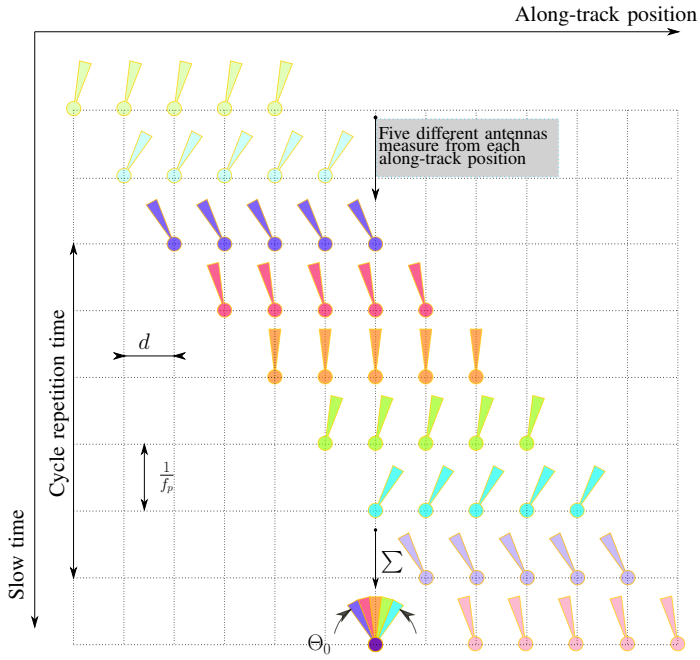

Fig. 1. Five channel schematic for design. Circles denote the phase-centre location while the angle denotes the direction of the transmit and receive beams.

As can be seen from the figure, if viewed vertically, at each sampling point, the system is configured to make 5 measurements with 5 different antenna patterns. If each of these antenna patterns has a beamwidth given by $\Theta/(M+1)$, then at each sampling point, the system scans over a total azimuth beamwidth of Θ. The reduced beamwidth at each sampling instant corresponds to a reduced required PRF for each channel according to

$$f_p \geq B_a/(M+1). \tag{1}$$

A. System design size

Consider the requirement for an azimuth resolution of δ_0. From fundamental SAR theory, for a classical stripmap mode, this corresponds to an antenna length given by [3]

$$L_0 = 2\delta_0, \tag{2}$$

which, in turn, corresponds to a required azimuth beamwidth of

$$\Theta_0 = \frac{\lambda}{2\delta_0}. \tag{3}$$

If this desired beamwidth is divided into $M+1$ parts of width

$$\Theta_M = \frac{\Theta_0}{M+1} = \frac{\lambda}{2(M+1)\delta_0}, \tag{4}$$

then each channel requires an antenna of length

$$L_M = 2(M+1)\delta_0. \tag{5}$$

The required PRF is given by

$$f_p = \frac{2v_s}{\lambda}\Theta_M = \frac{2v_s}{L_M} = \frac{v_s}{(M+1)\delta_0}, \tag{6}$$

which corresponds to a required two-way phase-centre separation of

$$d = (M+1)\delta_0. \tag{7}$$

Now, with a transmit antenna of length $L_M = 2(M+1)\delta_0$ and a receive antenna of the same length, the effective phase centre positions are given by multiples of $d = (M+1)\delta_0$. The total antenna length, as illustrated in figure 2, will be given by

$$L = (M+1)L_M = 2(M+1)^2\delta_0. \tag{8}$$

Let us examine what this means for a specific case of

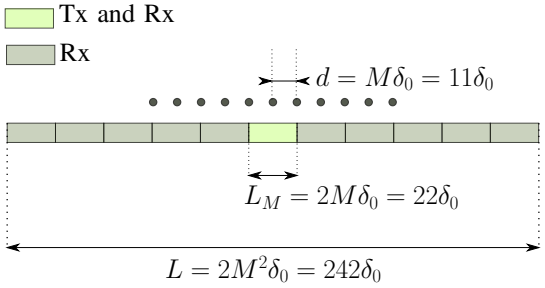

Fig. 2. Antenna Lengths to achieve desired resolution for an example 11 channel system for a desired resolution of δ_0.

$\delta_0 = 0.1$. As listed in table II, a traditional stripmap SAR would have to be 0.2 m in azimuth length to achieve this resolution. Additionally the required PRF would be $f_p = 75$ KHz for a satellite travelling at 7500 m/s which corresponds to a rather limited swath. On the other hand, with $M = 10$, the required PRF is $f_p = 6.818$ KHz which corresponds to a range-swath width of approximately 22 Km (minus any time needed for chirp transmission) which would be even larger in ground range.

The choice of $\delta_0 = 0.1, M = 10$ leads to an antenna of length 24.2 m with each subaperture having a length of 2.2 m. This antenna length of 24.2 m is only about 60% longer than RADARSAT-2.

TABLE II
SYSTEM PARAMETERS FOR $\delta_0 = 0.1$M AND $v_s = 7500$M/S.

M	L_M **m**	L **m**	f_p **Hz**	**Swath (slant-range Km)**
0	0.20	0.20	75000	2.00
2	0.60	1.80	25000	6.00
4	1.00	5.00	15000	10.00
6	1.40	9.80	10710	14.00
8	1.80	16.20	8330	18.00
10	**2.20**	**24.20**	**6810**	**22.00**
12	2.60	33.80	5760	26.00
14	3.00	45.00	5000	30.00

B. Traditional HRWS configuration and design

It is useful to examine the implication of utilising a traditional HRWS configuration that does not use a sequence of beams as proposed in this paper. With this design, $M+1$ channels transmit a wide beam that covers the desired range of angles corresponding to the desired resolution; see Figure 3. The spatial distribution of two-way phase-centres at each pulse again compensates for a lower PRF according to (6) [5].

To satisfy the spatial sampling requirement, the two-way phase-centre separation must be the same as with the proposed multi-beam design. This means that the receive antenna elements must be spaced by $2\delta_0$, giving a total receive antenna length of $2(M+1)\delta_0$ which is $(M+1)$ times shorter than the length proposed by the multi-beam design. This means that, on a pulse-by-pulse basis, the total receive area to capture reflected flux is reduced by a factor of $M+1$ resulting in a corresponding loss in SNR. For this reason, the multi-beam design is recommended.

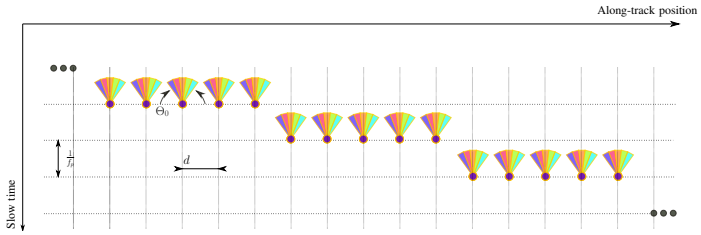

Fig. 3. Equivalent HRWS system.

III. Transmit antenna

Although the proposed design consists of $M+1$ subapertures, the requirements on the width of the transmit beam prevent transmission from the entire antenna. Transmission from the entire antenna would lead to a beam that is too narrow. Rather than route a finite power supply evenly across the entire antenna, one could instead supply the entirety of the available power only to the centre subaperture for transmission. Alternatively, one could transmit from the entire antenna, but with a spoiled pattern.

One advantage to the first approach is that only the centre subaperture requires the ability to transmit (as illustrated in figure 2), while the other subapertures can simply be passive receivers. Of course, if the system is to be used for other purposes, then it may not be desirable to limit transmit capability only to the centre subaperture.

Note that one can easily narrow the two-way beam by transmitting from a larger number of T/R modules. This may be desirable if the user wishes for the data to be sampled above the Nyquist rate.

IV. Signal processing algorithm

This section presents the promised third component of the improved SAR imaging capability; namely, the fundamentals of a suitable signal processing method. As we have already seen, the desired configuration impacts the design. The signal processing method presented in this section, on the other hand, is one of potentially several others, and its adoption does not place any restrictions upon the configuration or the design.

The previous material depends on a strict timing regime. A practical system may only operate with near-ideal timing conditions and this raises the questions of impact and how best to process the data under these conditions.

Even if timing conditions are perfect, the best approach to data processing is not entirely clear. A simple approach first concatenates the measurements from each beam into a uniformly-sampled time series and then transforms the data from the fast-time, slow-time domain into the fast-time Doppler domain. Given that, for each beam direction, the data correspond to different Doppler centroids, one could assign each response to different portions of the Doppler spectrum (or to different Doppler frequency bands). The union of these Doppler frequency bands corresponds to a wider Doppler spectrum and thereby to higher overall azimuth resolution. If the Doppler bands are non-overlapping, the concept of the union of the frequency bands is straight-forward. Optimal processing of Doppler bands that do overlap, however, requires a more rigorous approach. Optimal processing of data collected under non-ideal timing further calls for a flexible yet robust processing approach.

Given that processing should apply to very high-resolution systems, it is best that the approach be suitable for a wide-band system.

The derivation of an optimal processing approach would require more space than available for a letter publication. This section, therefore, only presents the final algorithm along with references to the derivation.

A. The measured signal

In continuous time, the signal from antenna m, beam n at fast time τ and slow time ξ is represented as

$$zz_{m,n}(\tau,\xi) = ss_{m,n}(\tau,\xi) + \nu\nu_{m,n}(\tau,\xi) \tag{9}$$

where $\nu\nu_{m,n}(\tau,\xi)$ represents white noise and $ss_{m,n}(\tau,\xi)$ the desired clutter signal. We introduce the vector signal

$$\mathbf{z}(\tau,\xi) = \begin{bmatrix} \begin{bmatrix} ss_{0,0}(\tau,\xi) \\ ss_{1,0}(\tau,\xi) \\ \vdots \\ ss_{M,0}(\tau,\xi) \end{bmatrix} \\ \begin{bmatrix} ss_{0,1}(\tau,\xi) \\ ss_{1,1}(\tau,\xi) \\ \vdots \\ ss_{M,1}(\tau,\xi) \end{bmatrix} \\ \vdots \\ \begin{bmatrix} ss_{0,N}(\tau,\xi) \\ ss_{1,N}(\tau,\xi) \\ \vdots \\ ss_{M,N}(\tau,\xi) \end{bmatrix} \end{bmatrix} + \boldsymbol{\nu}(\tau,\xi) \tag{10}$$

where $\boldsymbol{\nu}(\tau,\xi)$ is a vector of white noise values.

Due to the relationship between Doppler frequency and azimuth angle, the measured vector signal is, perhaps, most

readily processed in the frequency domain. As a simplification, this letter assumes that the two-way phase-centre positions of each channel are evenly aligned along the direction of motion so that each two-way phase centre is located at along-track position $md\hat{\mathbf{v}}_{\mathfrak{s}}(\xi)$, where $\hat{\mathbf{v}}_{\mathfrak{s}}(\xi)$ denotes the unit vector in the direction of the satellite velocity vector over slow-time. Without going into the derivation, we present the unambiguous frequency domain representation of the signal as

$$\mathcal{F}\{ss_{m,n}(\tau,\xi)\} = \mathcal{SS}_{m,n}(k_r,k_\chi) \tag{11}$$

where,

$$\mathcal{SS}_{m,n}(k_r,k_\chi) = e^{-i[md\kappa+nv_e/f_p]k_\chi}\mathcal{GG}_n(k_r,k_\chi). \tag{12}$$

The phase term at the front corresponds to spatial sampling delays from one channel to the next and temporal sampling delays from one beam to the next. The signal from each beam contains many terms that are conveniently separated into terms that correspond to the antenna pattern (or beam) and terms that correspond to the imaging geometry.

$$\mathcal{GG}_n(k_r,k_\chi) = \int \mathrm{D}_n[k_r,\hat{\mathbf{r}}(k_r,k_\chi,\phi)]v(k_r,k_\chi,\phi)\mathrm{d}\phi, \tag{13}$$

where the amplitude of the antenna pattern is given by $\mathrm{D}_n[k_r,\hat{\mathbf{r}}(k_r,k_\chi,\phi)]$ which depends on the direction of the beam through n, does **not** depend on the two-way phase-centre location (no m dependence) and also depends on the wavelength through k_r. The term that corresponds to the geometry and the reflectivity is given by

$$\begin{aligned} v(k_r,k_\chi,\phi) = C_0\mathcal{P}(k_{r'})\frac{(k_r^2-k_\chi^2)^{\frac{1}{4}}}{v_{\mathfrak{s}}k_r} \\ \int \frac{g[r,\chi_t,\phi]}{\sqrt{r}}e^{-i\chi_t k_\chi - ir\sqrt{k_r^2-k_\chi^2}}\mathrm{d}r\mathrm{d}\chi_t \end{aligned}, \tag{14}$$

where, $k_\chi = 2\pi f_\xi/v_e$, v_e represents the effective satellite velocity (relative) and f_ξ represents the slow-time Doppler frequency. Also $\kappa = v_e/v_s$, where v_s is the amplitude of the satellite velocity vector, $\mathbf{v}_{\mathfrak{s}}(\xi)$, and is assumed constant over ξ. The function, $g[r,\chi_t,\phi]$, represents the terrain reflectivity as a function of range, r from the radar, along-track position, χ_t and depression angle, ϕ. Note that the hyperbolic phase term, $\sqrt{k_r^2-k_\chi^2}$, may be insufficiently accurate for extremely high azimuth resolution [6]. In this case, a more accurate expression can be computed from the material in [9]. The look-direction vector in the 2D frequency domain is given by

$$\hat{\mathbf{r}}(k_r,k_\chi,\phi) = \frac{1}{k_r}\begin{bmatrix} -\kappa k_\chi \\ \cos\phi\sqrt{k_r^2-k_\chi^2} \\ \sqrt{\sin^2\phi[k_r^2-k_\chi^2]+k_\chi^2(1-\kappa^2)} \end{bmatrix}. \tag{15}$$

Finally, $\mathcal{P}(k_{r'})$ denotes the baseband frequency ($k_{r'}$) response of the pulsed waveform after processing for pulse compression, and C_0 is some constant. Derivation of the above material can be found in [9].

B. Multi-channel processing

Let

$$\mathbf{h}(k_r,k_\chi,\phi) = \begin{bmatrix} e^{-i0d_tk_\chi}\mathrm{D}_0[k_r,\hat{\mathbf{r}}(k_r,k_\chi,\phi)] & \begin{bmatrix} e^{-i0d_sk_\chi} \\ e^{-i1d_sk_\chi} \\ \vdots \\ e^{-iMd_sk_\chi} \end{bmatrix} \\ e^{-i1d_tk_\chi}\mathrm{D}_1[k_r,\hat{\mathbf{r}}(k_r,k_\chi,\phi)] & \begin{bmatrix} e^{-i0d_sk_\chi} \\ e^{-i1d_sk_\chi} \\ \vdots \\ e^{-iMd_sk_\chi} \end{bmatrix} \\ \vdots & \\ e^{-iNd_tk_\chi}\mathrm{D}_N[k_r,\hat{\mathbf{r}}(k_r,k_\chi,\phi)] & \begin{bmatrix} e^{-i0d_sk_\chi} \\ e^{-i1d_sk_\chi} \\ \vdots \\ e^{-iMd_sk_\chi} \end{bmatrix} \end{bmatrix}, \tag{16}$$

where, $d_t = v_e/f_p$ and $d_s = d\kappa$.

The sampled signal is gven by

$$\begin{aligned} \mathbf{Z}_s(k_r,k_\chi) &= \sum_l \int \mathbf{h}(k_r,k_\chi+lk_{\chi_p})v(k_r,k_\chi+lk_{\chi_p},\phi)\mathrm{d}\phi \\ &\quad + \boldsymbol{\nu}(k_r,k_\chi) \\ &= \int \mathbf{H}(k_r,k_\chi,\phi)\mathbf{v}(k_r,k_\chi,\phi)\mathrm{d}\phi + \boldsymbol{\nu}(k_r,k_\chi), \end{aligned} \tag{17}$$

where

$$\mathbf{H}(k_r,k_\chi,\phi) = \begin{bmatrix}\ldots & \mathbf{h}(k_r,k_\chi-k_{\chi_p},\phi) & \mathbf{h}(k_r,k_\chi,\phi) & \ldots\end{bmatrix}, \tag{18}$$

and

$$\mathbf{v}(k_r,k_\chi,\phi) = \begin{bmatrix} \vdots \\ v(k_r,k_\chi-k_{\chi_p},\phi) \\ v(k_r,k_\chi,\phi) \\ \vdots \end{bmatrix}, \tag{19}$$

and, where the spatial sampling frequency is given by

$$k_{\chi_p} = \frac{2\pi f_p}{(M+1)(N+1)v_e}. \tag{20}$$

Each component of $\mathbf{Z}_s(k_r,k_\chi)$ is undersampled in k_χ; however, by applying linear filters an unambiguous scalar spectrum of the signal may be reconstructed. Let us consider a single value of ϕ and apply a filtering matrix via $\mathbf{B}(k_r,k_\chi,\phi)\mathbf{H}(k_r,k_\chi,\phi) = \mathbf{D}(k_r,k_\chi,\phi)$. If the result, $\mathbf{D}(k_r,k_\chi,\phi)$, is diagonal, then we have constructed a mechanism to extract unambiguous signal components - we need only assign the elements of the vector

$$\mathbf{B}(k_r,k_\chi,\phi)\mathbf{H}(k_r,k_\chi,\phi)\mathbf{v}(k_r,k_\chi,\phi)+\mathbf{B}(k_r,k_\chi,\phi)\boldsymbol{\nu}(k_r,k_\chi) \tag{21}$$

to each band. As seen in the above, however, the noise component has also been filtered by this matrix and can possibly lead to degraded SNR. In addition to desiring a diagonal matrix (or as close as possible) for $\mathbf{D}(k_r,k_\chi,\phi)$, it is also fitting to select this matrix such that it has diagonal

elements given by the average of the antenna patterns, i.e. $D_{ll}(k_\chi) = \widetilde{\mathrm{D}}[k_r, \hat{\mathbf{r}}(k_r, k_\chi - lk_{\chi_p}, \phi)]$ where

$$\widetilde{\mathrm{D}}[k_r, \hat{\mathbf{r}}(k_r, k_\chi, \phi)] = \sqrt{\frac{1}{N+1}\sum_{n=0}^{N}\left|\mathrm{D}_n[k_r, \hat{\mathbf{r}}(k_r, k_\chi, \phi)]\right|^2}. \tag{22}$$

This desired antenna pattern has support over a wide range of azimuth angles and hence leads to a high-resolution signal.

As can be shown, the optimal filter matrix, in a mean-squared error sense, is given by

$$\mathbf{B}(k_r, k_\chi, \phi) = \mathbf{D}(k_r, k_\chi, \phi)\mathbf{H}^\dagger(k_r, k_\chi, \phi) \left[\mathbf{H}(k_r, k_\chi, \phi)\mathbf{H}^\dagger(k_r, k_\chi, \phi) + \frac{1-\varrho}{\varrho}\mathbf{R}_n(k_r, k_\chi, \phi)\right]^{-1}, \tag{23}$$

where $\mathbf{R}_n(k_r, k_\chi, \phi)$ is the noise covariance matrix.

C. Simulated Point Spread Function

To demonstrate the signal processing approach, this section generates a simulated signal using the design parameters of an 11-channel system. The simulation, with parameters listed in Table III, has been computed in Python with plots generated with Matplotlib. The simulator computes the back-folded signal for each of the 121 channels of data, computes the processing filters, applies the filters to the back-folded data and presents the amplitude of the reconstructed signal in the Doppler domain in Figure 4. The response in the Doppler domain shows the desired response across a region spanning 75 KHz with each local maximum in this region highlighting the response of each sub-beam. The simulator then azimuth compresses this reconstructed signal with a computed chirp and transforms the data back into the spatial domain to produce the Point Spread Function (PSF) shown in Figure 5. This figure illustrates that the system achieves the desired resolution with the response width less than 0.1 m at the -5 dB level. While the figure also shows a second set of sidelobes at -15 dB, it is assumed that these can be reduced by an appropriate choice of weighting on the antenna patterns.

TABLE III
SIMULATION PARAMETERS

f_p	6810 Hz
L_M	2.2 m
L	22 m
M	11
λ	0.031067 m
$\Delta\Theta_M$	0.809 deg

A test noise signal is also generated by the simulator. The SNR prior to filtering is compared with the SNR after filtering (but before azimuth compression) giving a change of about -0.4 dB. This shows that with the simulated parameters, the SNR does not change significantly.

In summary, the simulation demonstrates the suitability of the proposed signal processing algorithm and also shows how the generated PSF contains extra sidelobes that most likely result from the different shape of the signal response in the Doppler domain. If these sidelobes are intolerable, they can possibly be removed by modifying the phased-array beam tables; however, this is a topic for further research.

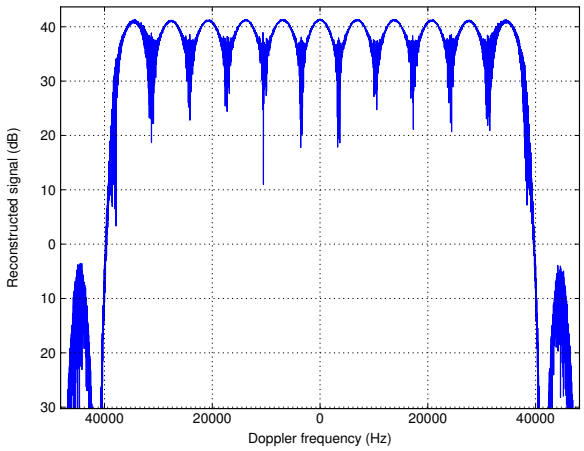

Fig. 4. Response of the reconstructed signal in the Doppler domain.

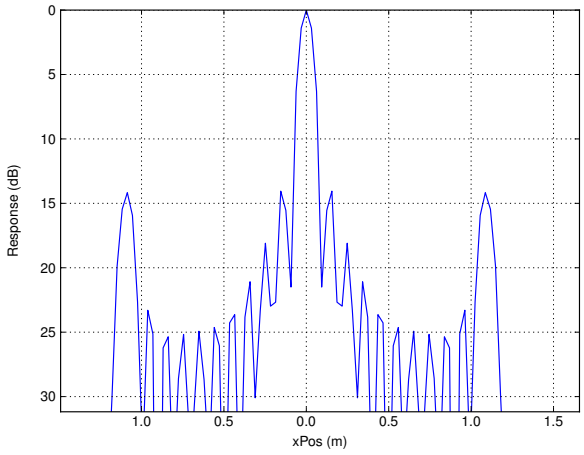

Fig. 5. Point Spread Function using the described processing method.

V. CONCLUSION

This letter proposes a system for improved space-based SAR imaging, describing the design, which is based upon a phased-array and an appropriate switching network to allow digitisation of multiple receive channels, the configuration, which imposes a rapid electronic beam switching capability upon the design, and a suitable signal processing algorithm to compute the high resolution imagery. The proposed configuration permits measurement of a relatively large swath in a Stripmap-like mode, thereby offering, theoretically, unlimited azimuth extent. On the other hand, as demonstrated by the test example of 10cm azimuth resolution considered throughout the paper, the resolution of the imagery can be even better than the highest resolution spotlight imagery available from current commercial systems.

Importantly, the state of current technology is sufficiently advanced to construct such a SAR system.

As a final important consideration, we note that the design does not preclude the use of other traditional measurement modes such as Spotlight, TOPS or ScanSAR. Further, it provides the flexibility to implement other advanced modes such as HRWS and Ground Moving Target Indication.

REFERENCES

[1] B. Brautigam, P. Rizzoli, C. Gonzalez, M. Weigt, D. Schrank, D. Schulze, and M. Schwerdt. SAR performance monitoring for TerraSAR-X mission. In *Geoscience and Remote Sensing Symposium (IGARSS), 2010 IEEE International*, pages 3454–3457, 2010.

[2] Diego Calabrese. DIscrete Stepped Strip (DI2S). In *EUSAR 2014; 10th European Conference on Synthetic Aperture Radar; Proceedings of*, pages 1–4, June 2014.

[3] I. G. Cumming and F. H. Wong. *Digital Processing of Synthetic Aperture Radar Data: Algorithms and Implementation*. Artech House Remote Sensing Library, Norwood, MA, 2005.

[4] Peter A Fox, Anthony P Luscombe, and Alan A Thompson. RADARSAT-2 SAR modes development and utilization. *Canadian journal of remote sensing*, 30(3):258–264, 2004.

[5] N. Gebert. *Multi-Channel Azimuth Processing for High-Resolution Wide-Swath SAR Imaging*. PhD thesis, University of Karlsruhe, 2009.

[6] J. Mittermayer, S. Wollstadt, P. Prats-Iraola, and R. Scheiber. The terrasar-x staring spotlight mode concept. *IEEE Transactions on Geoscience and Remote Sensing*, 52(6):3695–3706, June 2014.

[7] M. Porfilio, S. Serva, C. A. M. Fiorentino, and D. Calabrese. The acquisition modes of cosmo-skymed di seconda generazione: A new combined approach based on sar and platform agility. In *2016 IEEE International Geoscience and Remote Sensing Symposium (IGARSS)*, pages 2082–2085, July 2016.

[8] I. Sikaneta and C. Gierull. Phased-array beam-diversity with multiple channels for improved sar imaging. *IEEE Journal of Selected Topics in Applied Earth Observations and Remote Sensing*, 8(11):5106–5115, Nov 2015.

[9] I. C. Sikaneta and D. Cerutti-Maori. *Novel Radar Techniques and Applications*, chapter High-resolution wide-swath SAR. SciTech Publishing, Raleigh, 2017.